Supplementary Information
Frontiers of Earth Science

Understanding and Improving Yangtze River Basin Summer Precipitation Prediction Using an Optimal Multi-Physics Ensemble

Yang Zhao[1], Fengxue Qiao[2,3], Xin-Zhong Liang (✉)[4,5], and Jinhua Yu (✉)[6]

[1] Climate, Environment and Sustainability Center, Nanjing University of Information Science and Technology, Nanjing 210044, China

[2] Key Laboratory of Geographic Information Science, Ministry of Education, East China Normal University, Shanghai, 200241, China

[3] School of Geographic Sciences, East China Normal University, Shanghai, 200241, China

[4] Department of Atmospheric and Oceanic Science, University of Maryland, College Park, Maryland 20740, USA

[5] Earth System Science Interdisciplinary Center, University of Maryland, College Park, Maryland 20740, USA

[6] Key Laboratory of Meteorological Disaster, Ministry of Education (KLME) / Collaborative Innovation Center on Forecast and Evaluation of Meteorological Disasters (CIC-FEMD), Nanjing University of Information Science and Technology, Nanjing 210044, China

*_Corresponding author address:_ Department of Atmospheric and Oceanic Science, University of Maryland, College Park, MD 20740, USA; E-mail: xliang@umd.edu

*_Corresponding author address:_ Key Laboratory of Meteorological Disaster, Ministry of Education (KLME), Nanjing University of Information Science and Technology, Nanjing 210044, China; E-mail: jhyu@nuist.edu.cn

Section S1: Definition of circulation and its bias indices

The U200 bias index、the H200 bias index、the V850 or TPW bias index are respectively computed by taking the difference between the deviations of 200-hPa zonal wind、the 200-hPa geopotential height、the 850-hPa meridional wind or total precipitable water from ERA5 averaged over the core positive and/or negative correlation centers, as shown in the boxes in Fig. 4a, d, b or c. The circulation indices, similar to the circulation bias indices, are derived from the interannual variations of circulation monthly anomalies averaged over the core correlation centers, specified in the boxes in Fig. 5.

Section S2: Comprehensive ranking measure method

The comprehensive ranking measure (MR) (Jiang et al., 2015; Dong and Dong, 2021) is employed to comprehensively evaluate model performance in regional precipitation and associated circulation features (U200, V850, TPW, H200) in both mean conditions and interannual anomalies. For mean precipitation conditions, MR considers bias, spatial correlation, and root-mean-square errors (RMSE). For precipitation interannual anomalies, MR incorporates interannual correlation, RMSE, and the percentage of areas in the region with significant interannual correlations (SCA). For mean circulation conditions, MR takes into account biases in circulation bias indexes. For circulation interannual variations, MR is based on interannual correlations between precipitation and circulation indexes. MR is defined as:

$$\mathrm{MR} = 1 - \frac{1}{n \times m} \sum_{i=1}^{n} \mathrm{rank}_i, \qquad \text{(S1)}$$

where n is the number of skill metrics, m is the number of models, and $rank_i$ is the ranking of a specific model for the ith skill metric. Here, $rank_i$ is assigned sequentially from 1 to m. A lower rank value, or a value of MR closer to 1, indicates a better simulation performance by the model.

Section S3: Optimal ensemble and Bayesian Joint Probability calibrated ensemble

Informed by the aforementioned MR rankings, this study forms the optimal ensemble by selecting the most proficient CWRF configurations for simulating regional precipitation and associated circulations. This study also constructs BJP-calibrated ensemble by averaging the BJP calibration results from the top-performing individual CWRF configurations, with the purpose of reducing the YRB summer precipitation biases and exploring the potential to improve the interannual anomalies.

We introduce the Bayesian Joint Probability (BJP) model (Wang et al., 2009; Wang and Robertson, 2011) for post-processing climate precipitation simulations. The BJP calibration is exclusively applied to precipitation data from selected subsets of the most skillful CWRF physics configurations. The calibration covers three months across 36 summer seasons and includes all 1724 YRB grid cells, totaling 186,192 samples. The process employs a leave-one-year-out cross-validation approach (e.g., Schepen et al., 2020). The predictor "x" (simulated rainfall) and predictand "y" (observed rainfall) undergo a log-sinh transformation (Wang et al., 2012) for precipitation variables. We assume that the joint distribution of the transformed predictor $\tilde{x}$ and predictand $\tilde{y}$ follows a bivariate normal distribution, that is:

$$p(\tilde{x}, \tilde{y}) \sim N(\mu, \Sigma), \tag{S2}$$

Where μ and Σ are the mean vector and covariance matrix, respectively. The model parameters θ, comprising $\{\mu, \Sigma\}$, are estimated using Bayesian inference, with non-informative prior distributions defined for the model parameters. Posterior distributions for these parameters are derived by employing a Gibbs sampling approach, which generates 1,000 sampled parameter sets (Wang et al., 2019). The posterior predictive density for a new event is described by:

$$f(y|x) = p(y|x; x_D, y_D) = \int p(y|x; \theta)\, p(\theta|x_D, y_D) d\theta, \tag{S3}$$

Where (x_D, y_D) contains the predictor and predictand data used for parameter inference. Special procedures are incorporated to handle situations involving missing values and censored data (Wang and Robertson, 2011; Wang et al., 2019).

Section S4: Definition of the South Asian high index

The position of the ridge line in the South Asian high at 200 hPa is usually identified by the zero line of the westerly component. In this study, the ridge line's location is computed by averaging the latitudes of its intersections across nine longitudinal lines, ranging from 80°E to 120°E at 5-degree intervals. The eastern ridge point of the South Asian high is indicated by the longitude of its easternmost point at the 12,500 gpm contour. The high's latitudinal shifts are tracked through the ridge line, and its longitudinal movements through the position of the eastern ridge point.

Section S5: Physics dependence of YRB summer mean NRD and DRI biases

In terms of NRD (Figs. S2a and S3), ERI displays a notably large positive bias, exceeding 10-25 days over the YRB, which is the common "drizzling problem" observed in GCMs (Sun and Liang, 2020). Compared to ERI, ERA5 still shows positive bias but with improvements, including a 0.1 increase in PCC, a substantial 39% reduction in RMSE, and a reduced overestimation bias from 12.6 to 7.0 days. In comparison to ERI and ERA5, CTL significantly reduces the overestimation bias to just 2.2 days, and achieves a smaller RMSE of 9.0 days. However, this improvement is accompanied by a slight decrease in PCC by 0.02 compared to ERI. CWRF ECP members consistently resemble CTL, featuring correlations ranging from 0.55 to 0.69, RMSEs between 8.3 and 11.9 days, and biases spanning from -8.7 to 4.7 days. In particular, the CCCMA and CAML radiation schemes show significant improvement over CTL, producing higher PCCs, smaller RMSEs, and reduced overestimation bias down to 1.8 and 0.5, respectively. The Morrison and Morrison plus 3D aerosol microphysics schemes also demonstrated exceptional performance, showing similar PCCs and RMSEs compared to CTL, with overestimation biases of 3.1 and 2.7 days, respectively. As a result, CWRF's improvement in the underlying physical processes could effectively address the "drizzling problem" (Sun and Liang, 2020).

Conversely, configurations employing cumulus schemes other than ECP generally exhibit poorer performances. They display lower PCCs ranging from 0.04 to 0.15, larger RMSEs between 9.3 and 28.6 days, and larger negative biases averaging from 3.8 to 28.2 days. Specifically, the Tiedtke and Donner schemes both show significant deficits in rainy days by more than 35 days along coastal areas, leading to substantial underestimation of NRD averaging 24.9 and 28.2 days, respectively. The BMJ scheme exhibits a smaller area of negative bias, with the maximum exceeding 35 days in the upper reach of YRB, resulting in a significant underestimation of NRD averaging 14.9 days. The Emanuel scheme generates positive and negative biases in the upper and middle reaches, ultimately leading to a smaller average positive bias of 1.2 days due to the error cancelation.

For DRI (Figs. S2b and S4), ERI fails to capture the observed intensity center and underestimates intensity by more than 4 mm day^{-1} in both the upper and lower reaches. This results in a remarkably low PCC of -0.1, a large RMSE of 2.6 mm day^{-1}, and a systematic underestimation of 1.6 mm day^{-1} on average. Once again, ERA5 outperforms ERI, as shown by an increase in PCC by 0.77 and a 48% reduction in RMSE, but a slight overestimation of 0.4 mm day^{-1}. Compared to ERI, CTL also yields an evident increase in PCC by 0.46, a 10% reduction of RMSE, and a decreased underestimation bias to just 0.2 mm day^{-1}. Compared to CTL, most sensitivity test members generally produce higher PCCs (0.35-0.50), with RMSEs between 2.1 to 3.7 mm day^{-1}, and biases ranging from -2.9 to 0.1 mm day^{-1}. Two exceptions are using the ACM boundary layer scheme, and using the FuLiou radiation scheme, with the former producing a significantly lower correlation of 0.19 and the latter resulting in a much larger RMSE of 4.6 mm day^{-1} and a substantial underestimation of 4.0 mm day^{-1} on average.

Compared to using the ECP cumulus scheme in CTL, using the other cumulus schemes generally exhibit larger biases, lower PCCs, and larger RMSEs. Among them, the Donner, Tiedtke, and KFeta cumulus schemes all systematically overestimate DRI, with Donner having the largest positive bais of 10.8 mm day^{-1}, and KFeta having the positive bias of 6 mm day^{-1} and a substantial 200% increase in RMSE, but a 0.02 increase in PCC. On the other hand, the other three schemes (NSAS, Grell, BMJ) systematically underestimate DRI, with NSAS having an increased PCC by 0.11 and a reduced RMSE by 6%, but a relatively smaller underestimation by 1.4 mm day^{-1}.

Section S6: Comparison of BMPE and BMPE-bjp

It shows that BMPE-bjp remarkably outperforms BMPE in bias correction of the climate summer mean precipitation as expected by design, reaching a correlation of 1.0 and a smaller RMSE of 0.1 mm day^{-1}, even surpassing ERA5 and ERI (Fig. S5a). Nevertheless, it still maintains a small average dry bias of 0.09 mm day^{-1}, with a sharp frequency peak centered near -0.1 mm day^{-1} (Fig. S5b). However, BMPE-bjp worsens the skill in capturing YRB precipitation interannual anomalies, with a shift of the frequency peak to 0.31 with a more

flattened pattern, and large SCA reductions from 43.2% of CTL and 69.7% of BMPE to only 38.3%, particularly in regions to the north of the Yangtze River (Fig. S6a, b). The performance of BMPE-bjp is inferior to BMPE, reducing the interannual correlation by 0.13 and increasing RMSE by 7% (Fig. S6c). Figure S7 depicts the correlations between interannual anomalies of YRB precipitation and circulation features over the observed teleconnected area. Compared to CWRF CTL (Figs. 7 and 12), BMPE more accurately captures observed circulation teleconnections for U200, TPW, and H200, showing correlations of (0.42, 0.68, 0.39) that closely align with observations (0.42, 0.63, 0.38). However, for V850, BMPE exhibits a relatively higher correlation (0.51) than CTL, further deviating from the observed value (0.44). In contrast, BMPE-bjp exhibits poorer performance, displaying slightly stronger correlations with U200 (0.43) and TPW (0.70), but notably lower correlations with V850 (0.35). The results suggest that BMPE shows superiority over BMPE-bjp in capturing the linkage between precipitation and circulation, thereby improving the model's capability in reproducing the interannual precipitation anomalies in YRB.

Figures:

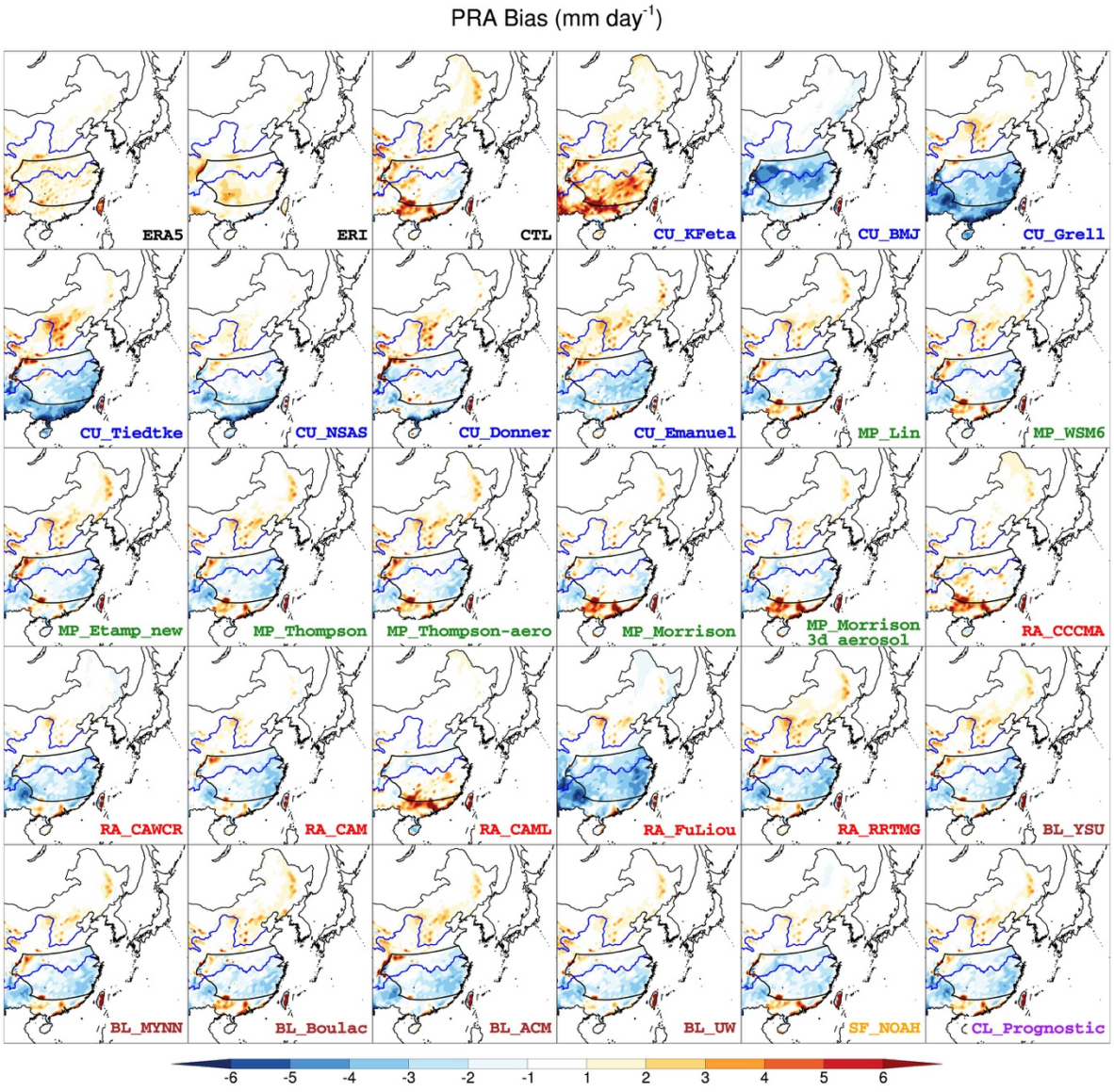

Fig. S1. Geographic distributions of 1980-2015 mean summer average precipitation amount (PRA) biases of ERA5 and ERI, and 28 different CWRF physics configurations from observations obtained. Outlined are the boundaries of YRB for the area of interest.

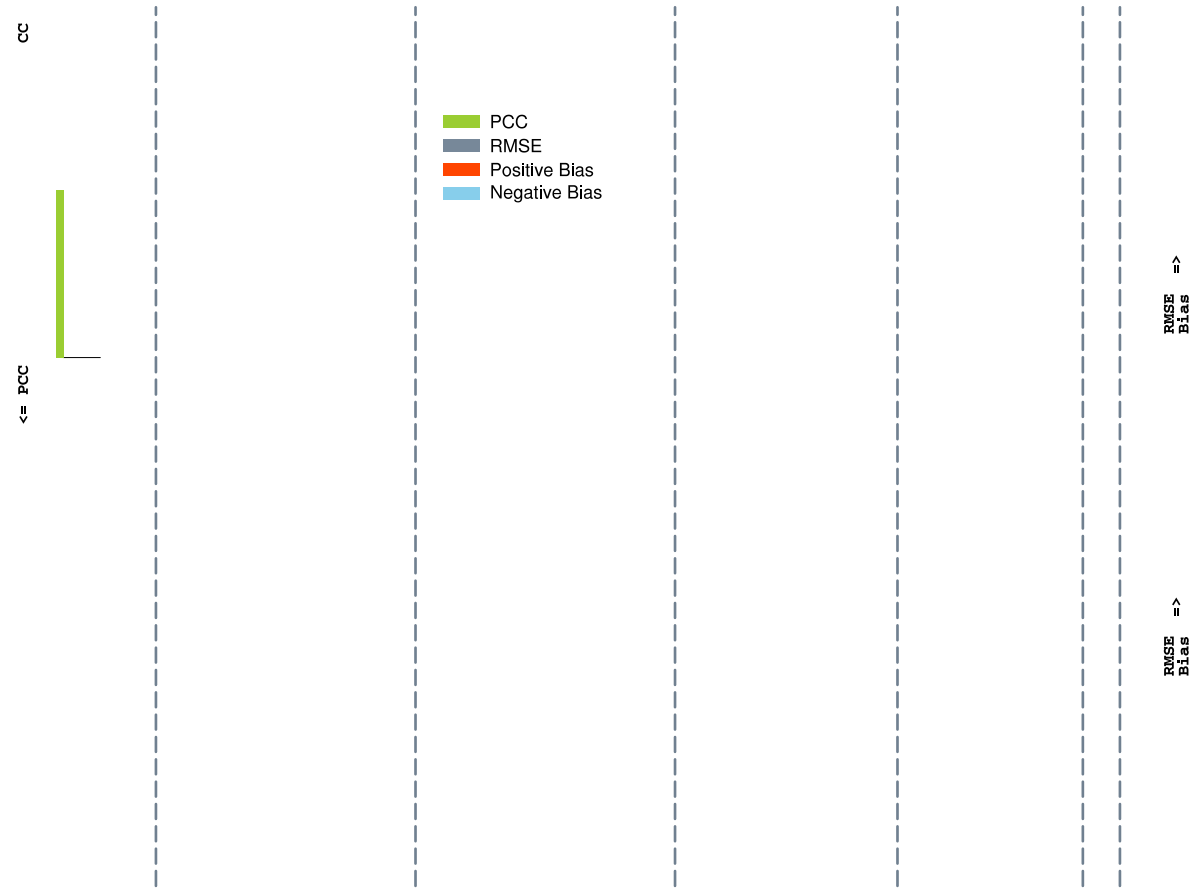

Fig. S2. The spatial pattern correlation coefficient (PCC), RMS error (RMSE), and average bias (Bias) between observations and ERA5, ERI, and 28 CWRF physics configurations for 1980-2015 mean summer average (a) number of rainy days (NRD, day) and (b) daily rainfall intensity (DRI, mm day^{-1}) over the YRB. Hatches denote statistically significant differences at the 95% significance level.

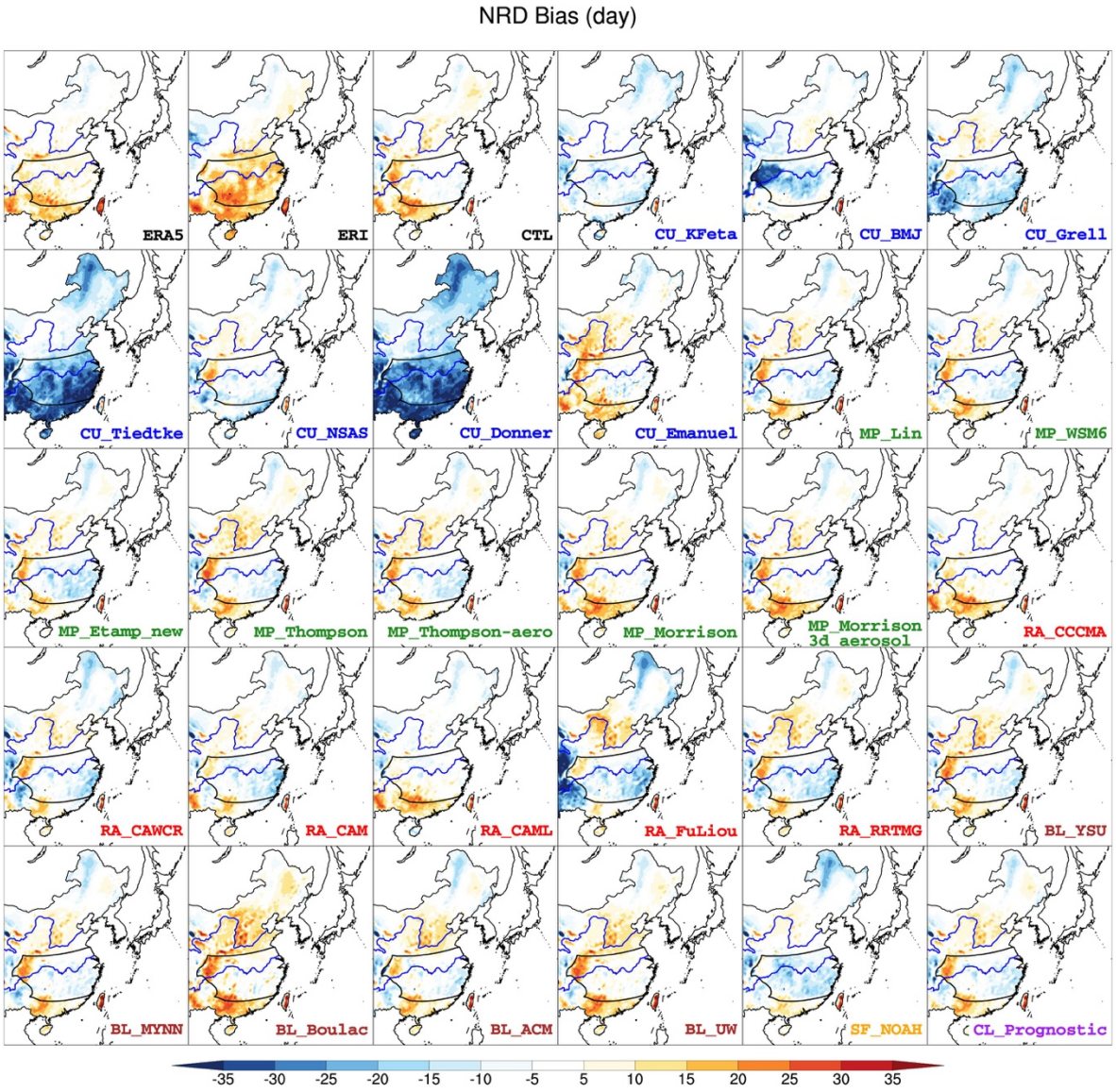

Fig. S3. Same as Fig. S1 except for the number of rainy days (NRD).

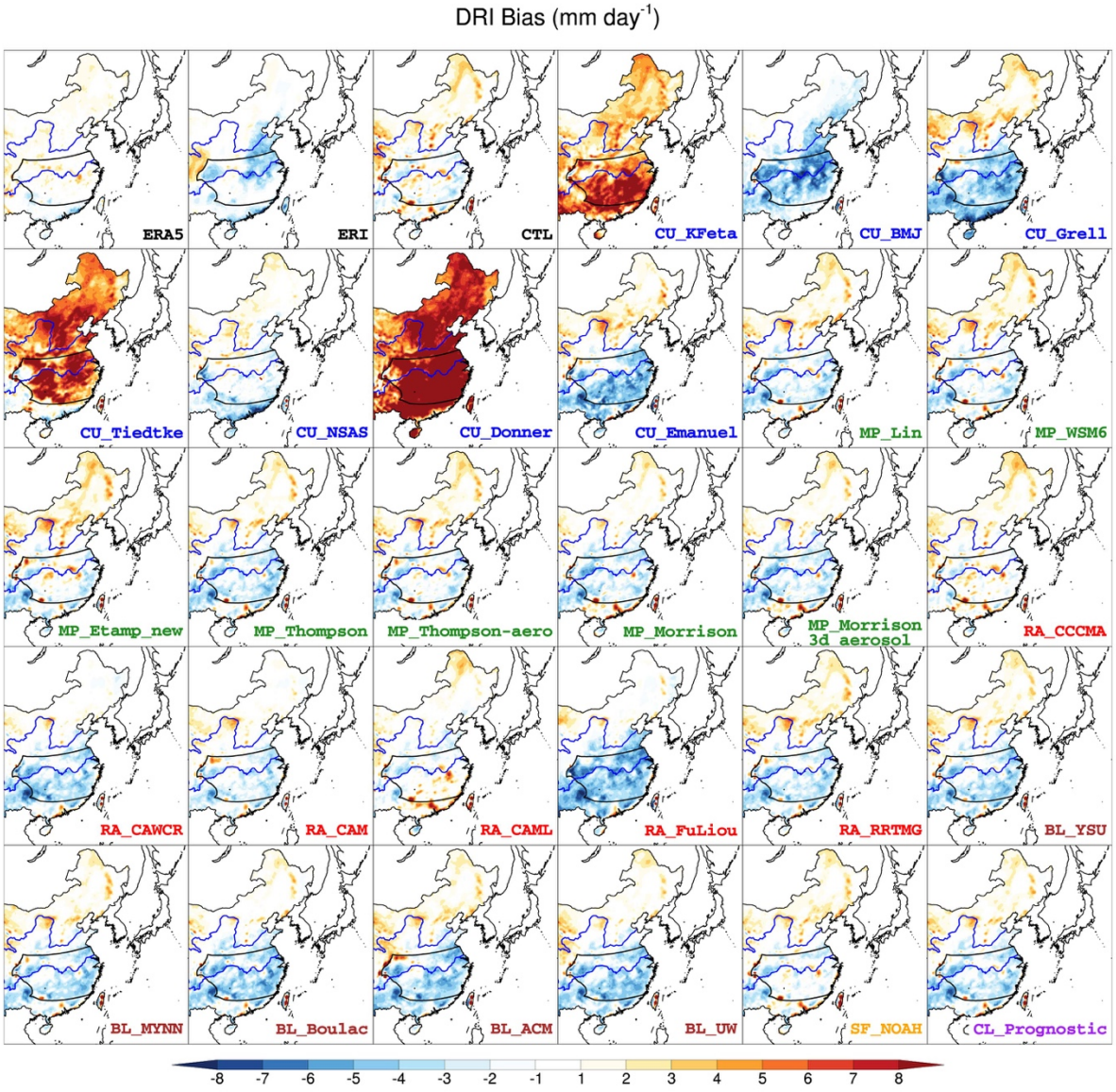

Fig. S4. Same as Fig. S1 except for the daily rainfall intensity (DRI).

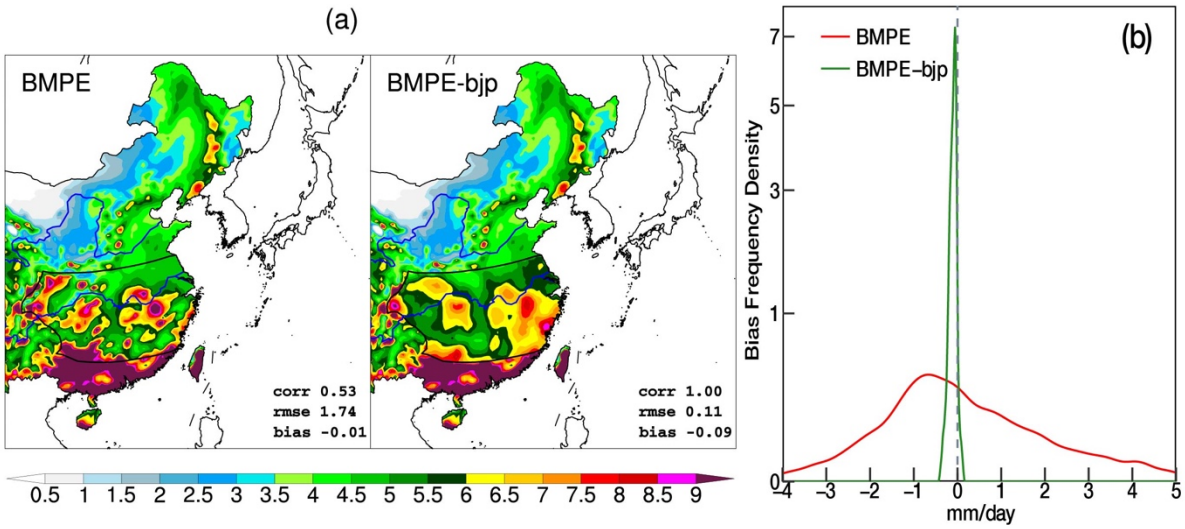

Fig. S5. (a) Spatial distributions of summer average precipitation as CWRF best multi-physics ensemble (BMPE) and BJP-calibrated ensemble (BMPE-bjp). Listed with the corresponding spatial pattern correlation, RMS error (rmse) and bias over the YRB compared with observations. (b) bias frequency density distributions over the YRB.

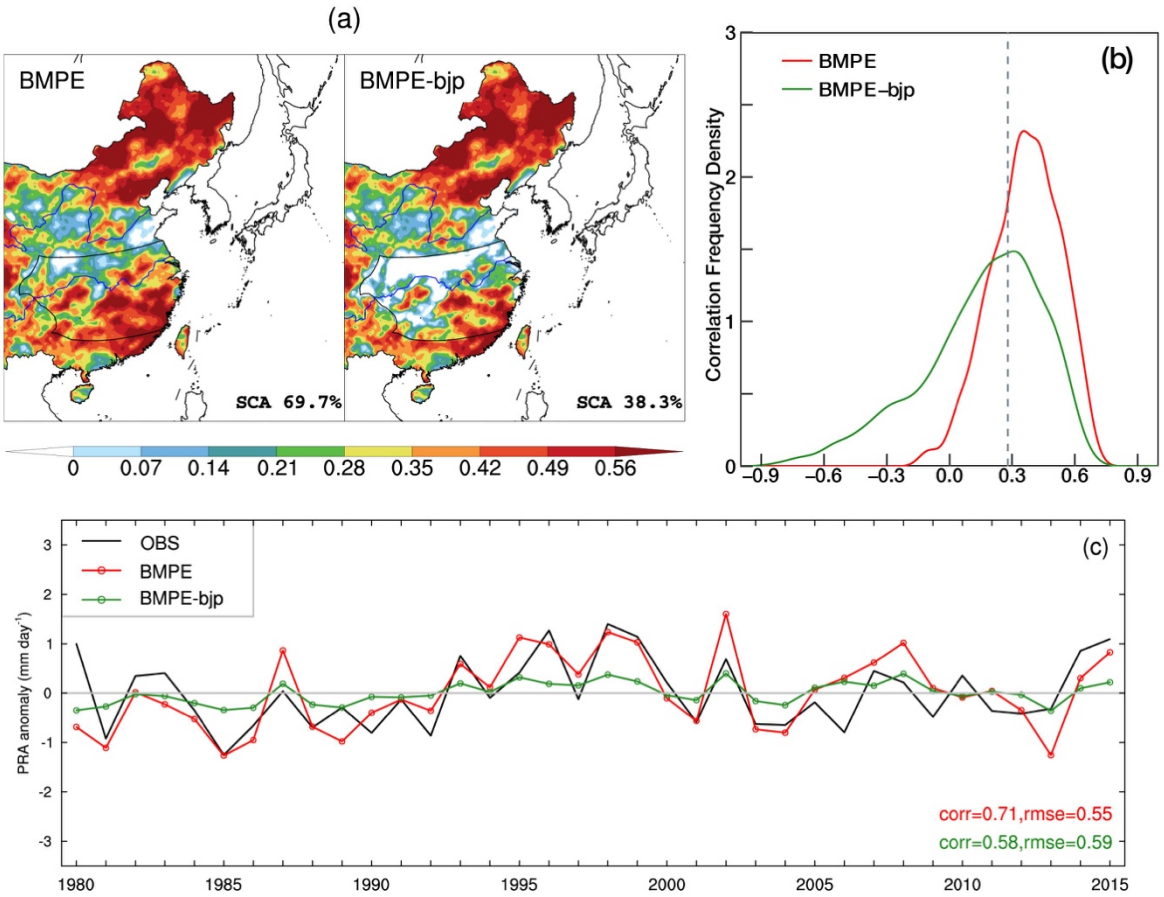

Fig. S6. CWRF BMPE and BMPE-bjp simulated (a) interannual correlations of summer

precipitation with observations, along with the percentage of basin areas that have significant interannual correlations (SCA). (b) frequency density functions of correlations at all CWRF grids within the YRB. Correlations above 0.28 marked by the vertical line are statistically significant at the 95% significance level, determined by a one-tail Student's t-test. (c) YRB-average precipitation interannual anomalies, along with their interannual correlation (corr) and RMS error (rmse) against observations.

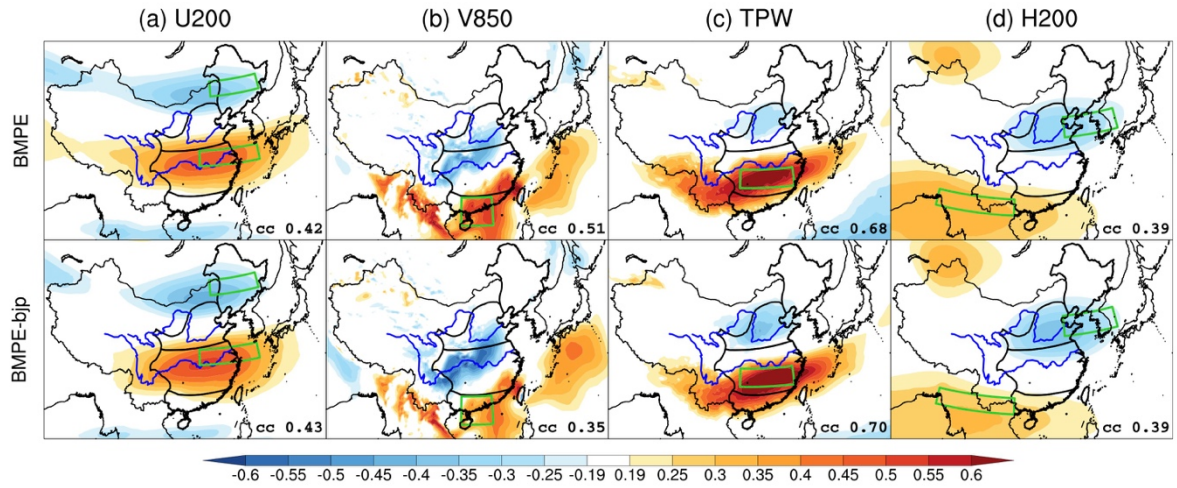

Fig. S7. Spatial distribution of correlations between the interannual anomalies of the YRB-average summer monthly precipitation and pointwise circulation features (U200, V850, TPW, H200) among CWRF BMPE and BMPE-bjp. Listed are the corresponding interannual correlations between the YRB-average summer monthly precipitation and circulation features averaged over the observed teleconnected area.

Table:

Table S1 Summary of the CWRF physical parameterization schemes used in this study

Physical processes	Run	Parameterizations	References
Cumulus (CU)	CTL	ECP	Grell and Dévényi (2002), Liang et al. (2012), Qiao and Liang (2015, 2016, 2017)
	E1	KFeta	Kain and Fritsch (1993), Kain (2004)
	E2	BMJ	Betts and Miller (1986), Janjić (1994, 2000)
	E3	Grell	Grell (1993), Grell and Dévényi (2002)
	E4	Tiedtke	Tiedtke (1989), Nordeng (1994)
	E5	NSAS	Han and Pan (2011)
	E6	Donner	Donner (1993), Donner et al. (2001)
	E7	Emanuel	Emanuel and Živković-Rothman (1999)
Microphysics (MP)	CTL	GSFCGCE	Tao et al. (2003)
	E8	Lin	Lin et al. (1983), Chen and Sun (2002)
	E9	WSM6	Hong and Lim (2006)
	E10	Etamp new	Rogers et al. (2001)
	E11	Thompson	Thompson et al. (2004, 2008)
	E12	Thompson-aero	Thompson and Eidhammer (2014)
	E13	Morrison	Morrison et al. (2009), Morrison and Milbrandt (2010, 2015)
	E14	Morrison+3d aerosol	Morrison microphysics scheme with aerosol mass loadings and optical properties or observed (Liang and Zhang, 2013)
Radiation (RA)	CTL	GSFCLXZ	Chou and Suarez (1999), Chou et al. (2001)
	E15	CCCMA	Li and Barker (2005), Li et al. (2005), Li and Shibata (2006)
	E16	CAWCR	Sun and Rikus (1999), Sun (2008)
	E17	CAM	Collins et al. (2004)
	E18	CAML	CAM radiation scheme as implemented by Liang together with the diagnostic cloud cover scheme of Xu and Randall (1996)
	E19	FuLiou	Fu and Liou (1992, 1993)
	E20	RRTMG	Iacono et al. (2008)
Boundary layer (BL)	CTL	CAM3	Holtslag and Boville (1993), Liang et al. (2012)
	E21	YSU	Hong and Lim (2006)
	E22	MYNN	Nakanishi and Niino (2006, 2009)
	E23	Boulac	Bougeault and Lacarrere (1989)
	E24	ACM	Pleim (2007) with updated MOL calculation refer to WRF3.7.1
	E25	UW	Park and Bretherton (2009)
Surface (SF)	CTL	CSSP	Dai et al. (2003, 2004), Liang et al. (2005a, b), Choi et al. (2007, 2013), Oleson et al. (2008), Choi and Liang (2010), Yuan and Liang (2011), Xu et al. (2014), Choi et al. (2015)
	E26	NOAH	Ek et al. (2003), Niu et al. (2011), Yang et al. (2011)
Cloud (CL)	CTL	Xu and Randall	Xu and Randall (1996), Liang et al. (2004)
	E27	Prognostic	Wilson et al. (2008)

Reference:

Betts A, Miller M (1986). A new convective adjustment scheme. Part II: Single column tests using GATE wave, BOMEX, ATEX and arctic air-mass data sets. Q J R Meteorolog Soc, 112: 693-709.

Bougeault P, Lacarrere P (1989). Parameterization of orography-induced turbulence in a mesobeta--scale model. Mon Weather Rev, 117: 1872-1890.

Chen S-H, Sun W-Y (2002). A one-dimensional time dependent cloud model. J Meteorolog Soc Jpn, 80: 99-118.

Choi H I, Kumar P, Liang X-Z (2007). Three-dimensional volume-averaged soil moisture transport model with a scalable parameterization of subgrid topographic variability. Water Resour Res, 43: W04414.

Choi H I, Liang X-Z (2010). Improved terrestrial hydrologic representation in mesoscale land surface models. J Hydrometeorol, 11: 797-809.

Choi H I, Liang X-Z, Kumar P (2013). A conjunctive surface–subsurface flow representation for mesoscale land surface models. J Hydrometeorol, 14: 1421-1442.

Choi I-J, Jin E K, Han J-Y, Kim S-Y, Kwon Y (2015). Sensitivity of diurnal variation in simulated precipitation during East Asian summer monsoon to cumulus parameterization schemes. J Geophys Res Atmos, 120: 11,971-911,987.

Chou M-D, Suarez M J (1999). A solar radiation parameterization for atmospheric studies. National Aeronautics and Space Administration, Goddard Space Flight Center …,

Chou M-D, Suarez M J, Liang X-Z, Yan M M-H, Cote C (2001). A thermal infrared radiation parameterization for atmospheric studies.

Collins W D, Rasch P J, Boville B A, Hack J J, McCaa J R, Williamson D L, Kiehl J T, Briegleb B, Bitz C, Lin S-J (2004). Description of the NCAR community atmosphere model (CAM 3.0). NCAR Tech. Note NCAR/TN-464+ STR, 226.

Dai Y, Zeng X, Dickinson R E, Baker I, Bonan G B, Bosilovich M G, Denning A S, Dirmeyer P A, Houser P R, Niu G (2003). The common land model. Bull Am Meteorol Soc, 84: 1013-1024.

Dai Y, Dickinson R E, Wang Y-P (2004). A two-big-leaf model for canopy temperature, photosynthesis, and stomatal conductance. J Clim, 17: 2281-2299.

Dong T, Dong W (2021). Evaluation of extreme precipitation over Asia in CMIP6 models. Clim Dyn, 57: 1751-1769.

Donner L (1993). A cumulus parameterization including mass fluxes, vertical momentum dynamics, and mesoscale effects. J Atmos Sci, 50(6): 889-906.

Donner L, Seman C, Hemler R, Fan S-M (2001). A cumulus parameterization including mass fluxes, convective vertical velocities, and mesoscale effects: Thermodynamic and hydrological aspects in a general circulation model. J Clim, 14: 3444-3463.

Ek M, Mitchell K, Lin Y, Rogers E, Grunmann P, Koren V, Gayno G, Tarpley J (2003). Implementation of Noah land surface model advances in the National Centers for Environmental Prediction operational mesoscale Eta model. J Geophys Res Atmos, 108: D22.

Emanuel K A, Živković-Rothman M (1999). Development and evaluation of a convection scheme for use in climate models. J Atmos Sci, 56: 1766-1782.

Fu Q, Liou K (1992). On the correlated k-distribution method for radiative transfer in nonhomogeneous atmospheres. J Atmos Sci, 49: 2139-2156.

Fu Q, Liou K (1993). Parameterization of the radiative properties of cirrus clouds. J Atmos Sci, 50: 2008-2025.

Grell G (1993). Prognostic evaluation of assumptions used by cumulus parameterizations. Mon Weather Rev, 121(3): 764-787.

Grell G, Dévényi D (2002). A generalized approach to parameterizing convection combining ensemble and data assimilation. Geophys Res Lett, 29: 38-41.

Han J, Pan H-L (2011). Revision of convection and vertical diffusion schemes in the NCEP global forecast system. Weather Forecasting, 26: 520-533.

Holtslag A, Boville B (1993). Local versus nonlocal boundary-layer diffusion in a global climate model. J Clim, 6: 1825-1842.

Hong S Y, Lim J O (2006). The WRF single-moment 6-class microphysics scheme (WSM6). J Korean Meteor Soc, 42: 129-151.

Iacono M J, Delamere J S, Mlawer E J, Shephard M W, Clough S A, Collins W D (2008). Radiative forcing by long-lived greenhouse gases: Calculations with the AER radiative transfer models. J Geophys Res Atmos, 113: 13103.

Janjić Z (1994). The step-mountain eta coordinate model: further development of the convection, viscous sublayer, and turbulent closure schemes. Mon Weather Rev, 122: 927-945.

Janjić Z (2000). Comments on “Development and Evaluation of a Convection Scheme for Use in Climate Models”. J Atmos Sci, 57(21): 3686.

Jiang Z, Li W, Xu J, Li L (2015). Extreme precipitation indices over China in CMIP5 models. Part I: Model evaluation. J Clim, 28: 8603-8619.

Kain J, Fritsch J (1993). Convective parameterization for mesoscale models: The Kain-Fritsch scheme. The representation of cumulus convection in numerical models. Springer, pp 165-170.

Kain J S (2004). The Kain - Fritsch convective parameterization: An update. J Appl Meteorol, 43: 170-181.

Li J, Dobbie S, Räisänen P, Min Q (2005). Accounting for unresolved clouds in a 1-D solar radiative-transfer model. Q J R Meteorolog Soc, 131: 1607-1629.

Li J, Barker H (2005). A radiation algorithm with correlated-k distribution. Part I: Local thermal equilibrium. J Atmos Sci, 62: 286-309.

Li J, Shibata K (2006). On the effective solar pathlength. J Atmos Sci, 63: 1365-1373.

Liang X-Z, Li L, Kunkel K E, Ting M, Wang J X (2004). Regional climate model simulation of US precipitation during 1982–2002. Part I: Annual cycle. J Clim, 17: 3510-3529.

Liang X-Z, Choi H I, Kunkel K E, Dai Y, Joseph E, Wang J X, Kumar P (2005a). Surface boundary conditions for mesoscale regional climate models. Earth Interact, 9: 1-28.

Liang X-Z, Xu M, Gao W, Kunkel K, Slusser J, Dai Y, Min Q, Houser P R, Rodell M, Schaaf C B (2005b). Development of land surface albedo parameterization based on Moderate Resolution Imaging Spectroradiometer (MODIS) data. J Geophys Res Atmos, 110.

Liang X-Z, Xu M, Yuan X, Ling T, Choi H, Zhang F, Chen L, Liu S, Su S, Qiao F, He Y, Wang J, Kunkel K, Gao W, Joseph E, Morris V, Yu T-W, Dudhia J, Michalakes J (2012). Regional Climate-Weather Research and Forecasting Model (CWRF). Bull Am Meteorol Soc, 93: 1363-1387.

Liang X-Z, Zhang F (2013). The cloud–aerosol–radiation (CAR) ensemble modeling system. Atmos Chem Phys, 13: 8335-8364.

Lin Y-L, Farley R, Orville H (1983). Bulk parameterization of the snow field in a cloud model. J Appl Meteorol, 22: 1065-1092.

Morrison H, Thompson G, Tatarskii V (2009). Impact of cloud microphysics on the development of trailing stratiform precipitation in a simulated squall line: Comparison of one-and two-moment schemes. Mon Weather Rev, 137: 991-1007.

Morrison H, Milbrandt J (2010). Comparison of two-moment bulk microphysics schemes in idealized supercell thunderstorm simulations. Mon Weather Rev, 139: 1103–1130.

Morrison H, Milbrandt J A (2015). Parameterization of cloud microphysics based on the prediction of bulk ice particle properties. Part I: Scheme description and idealized tests. J Atmos Sci, 72: 287-311.

Nakanishi M, Niino H (2006). An improved Mellor–Yamada level-3 model: Its numerical stability and application to a regional prediction of advection fog. Boundary Layer Meteorol, 119: 397-407.

Nakanishi M, Niino H (2009). Development of an improved turbulence closure model for the atmospheric boundary layer. J Meteorolog Soc Jpn, Ser. II 87: 895-912.

Niu G Y, Yang Z L, Mitchell K E, Chen F, Ek M B, Barlage M, Kumar A, Manning K, Niyogi D, Rosero E (2011). The community Noah land surface model with multiparameterization options (Noah-MP): 1. Model description and evaluation with local-scale measurements. J Geophys Res Atmos, 116: :D12109.

Nordeng T (1994). Extended versions of the convective parametrization scheme at ECMWF and their impact on the mean and transient activity of the model in the tropics. Research

Department Technical Memorandum, 206: 1-41.

Oleson K, Niu G Y, Yang Z L, Lawrence D, Thornton P, Lawrence P, Stöckli R, Dickinson R, Bonan G, Levis S (2008). Improvements to the Community Land Model and their impact on the hydrological cycle. J Geophys Res Biogeosci, 113.

Park S, Bretherton C S (2009). The University of Washington shallow convection and moist turbulence schemes and their impact on climate simulations with the Community Atmosphere Model. J Clim, 22: 3449-3469.

Pleim J E (2007). A combined local and nonlocal closure model for the atmospheric boundary layer. Part I: Model description and testing. J Appl Meteorol Climatol, 46: 1383-1395.

Qiao F, Liang X-Z (2015). Effects of cumulus parameterizations on predictions of summer flood in the Central United States. Clim Dyn, 45: 727-744.

Qiao F, Liang X-Z (2016). Effects of cumulus parameterization closures on simulations of summer precipitation over the United States coastal oceans. J Adv Model Earth Syst, 8: 764-785.

Qiao F, Liang X-Z (2017). Effects of cumulus parameterization closures on simulations of summer precipitation over the continental United States. Clim Dyn, 49: 225-247.

Rogers E, Black T, Ferrier B, Lin Y, Parrish D, DiMego G (2001). Changes to the NCEP Meso Eta Analysis and Forecast System: Increase in resolution, new cloud microphysics, modified precipitation assimilation, modified 3DVAR analysis. NWS Tech Proced Bull, 488: 15.

Schepen A, Everingham Y, Wang Q J (2020). On the joint calibration of multivariate seasonal climate forecasts from GCMs. Mon Weather Rev, 148: 437-456.

Sun C, Liang X-Z (2020). Improving US extreme precipitation simulation: Sensitivity to physics parameterizations. Clim Dyn, 54: 4891-4918.

Sun Z, Rikus L (1999). Parametrization of effective sizes of cirrus‐cloud particles and its verification against observations. Q J R Meteorolog Soc, 125: 3037-3055.

Sun Z (2008). Development of the Sun-Edwards-Slingo radiation scheme (SES2).

Tao W-K, Starr D, Hou A, Newman P, Sud Y (2003). A cumulus parameterization workshop. Bull Am Meteorol Soc, 84: 1055-1062.

Thompson G, Rasmussen R M, Manning K (2004). Explicit forecasts of winter precipitation using an improved bulk microphysics scheme. Part I: Description and sensitivity analysis. Mon Weather Rev, 132: 519-542.

Thompson G, Field P R, Rasmussen R M, Hall W D (2008). Explicit forecasts of winter precipitation using an improved bulk microphysics scheme. Part II: Implementation of a new snow parameterization. Mon Weather Rev, 136: 5095-5115.

Thompson G, Eidhammer T (2014). A study of aerosol impacts on clouds and precipitation development in a large winter cyclone. J Atmos Sci, 71: 3636-3658.

Tiedtke M (1989). A comprehensive mass flux scheme for cumulus parameterization in large-scale models. Mon Weather Rev, 117: 1779-1800.

Wang Q, Robertson D, Chiew F (2009). A Bayesian joint probability modeling approach for seasonal forecasting of streamflows at multiple sites. Water Resour Res, 45: W05407.

Wang Q, Robertson D (2011). Multisite probabilistic forecasting of seasonal flows for streams with zero value occurrences. Water Resour Res, 47: W02546.

Wang Q, Shrestha D L, Robertson D, Pokhrel P (2012). A log-sinh transformation for data normalization and variance stabilization. Water Resour Res, 48.

Wang Q J, Shao Y, Song Y, Schepen A, Robertson D E, Ryu D, Pappenberger F (2019). An evaluation of ECMWF SEAS5 seasonal climate forecasts for Australia using a new forecast calibration algorithm. Environmental Modelling & Software, 122: 104550.

Wilson D R, Bushell A C, Kerr-Munslow A M, Price J D, Morcrette C J, Bodas-Salcedo A (2008). PC2: A prognostic cloud fraction and condensation scheme. II: Climate model simulations. Q J R Meteorolog Soc, 134: 2109-2125.

Xu K-M, Randall D A (1996). A semiempirical cloudiness parameterization for use in climate models. J Atmos Sci, 53: 3084-3102.

Xu M, Liang X-Z, Samel A, Gao W (2014). MODIS consistent vegetation parameter specifications and their impacts on regional climate simulations. J Clim, 27: 8578-8596.

Yang Z L, Niu G Y, Mitchell K E, Chen F, Ek M B, Barlage M, Longuevergne L, Manning K, Niyogi D, Tewari M (2011). The community Noah land surface model with multiparameterization options (Noah-MP): 2. Evaluation over global river basins. J Geophys Res Atmos, 116.

Yuan X, Liang X-Z (2011). Evaluation of a Conjunctive Surface–Subsurface Process Model (CSSP) over the contiguous United States at regional–local scales. J Hydrometeorol, 12: 579-599.